Manuscript (double-spaced and continuously LINE and PAGE numbered)

Click here to view linked References

Can we estimate flood frequency with point-process spatial-temporal rainfall models?

Yuting Chen[1], Athanasios Paschalis[1], Li-Pen Wang[1], Christian Onof[1]

[1]Department of Civil and Environmental Engineering, Imperial College London, London, UK.

Corresponding author: Yuting Chen (yuting.chen17@imperial.ac.uk)

Abstract

Stochastic rainfall models are commonly used in practice for long-term flood risk management. One of the most widely used model types is based on point processes. Despite the widespread use of such models, whether their known simplifications in describing the space-time structure of rainfall will affect the accuracy of flood estimation has not been quantified. In this study, we quantify the biases introduced by the rainfall model limitations to flood estimates in two medium-sized river catchments (717 km^2 and 844 km^2) in the South East of the UK. To achieve this, we used nine years of hourly radar rainfall data, a dense network of hourly rain gauges, a spatial-temporal rainfall stochastic model based on point processes, and a fully distributed hydrological model. We modelled the corresponding catchment water dynamics using observed and simulated hourly rainfall and then assessed whether the errors introduced by the stochastic model will propagate in the river flow dynamics. Our results show that the stochastic rainfall model properly captures the point-scale rainfall statistics, including point extremes and the cross-site spatial correlations. However, the model results in a bias on extremes of areal statistics, including an overestimation of the areal reduction factor, extreme areal mean precipitation, and the areal fraction of rain (wet area ratio). Using this as input for continuous hydrological simulations, we find that the flow duration curves are well preserved, particularly in the high flow seasons (relative bias is less than 7%). The model also reproduces well the flood frequency curves at a daily scale with an averaged relative bias of 0.36-16.9% at 10-year return levels, confirming its ability to infer the long-term flood risk for medium-sized catchments. However, the summer-season hourly peak discharge is highly overestimated with a relative bias of over 163.5% at the same return level. The overestimation in summer hourly peak discharge is

explained by the dominating convective systems in summer and the misrepresented spatial structure in the model.

1 Introduction

Rainfall variability in both space and time is crucial to properly quantify the magnitude and uncertainty of streamflow (Cristiano et al., 2017; Faurès et al., 1995; Paschalis et al., 2014a). The temporal scale of the underlying hydrological processes of interest determines the temporal scale of required rainfall data. For example, sub-hourly resolution is required for urban catchments (Ochoa-Rodriguez et al., 2015) and hourly resolution is required for the larger river catchments (Melsen et al., 2016). In addition to the importance of temporal resolution, spatial variability of rainfall has been also highlighted in recent decades, mainly in terms of spatial resolution (Nicótina et al., 2008) and storm advection (Ran et al., 2012; Ruiz-Villanueva et al., 2012; Seo et al., 2012). The sensitivity of streamflow to rainfall patterns is catchment-dependent, rainfall-event-dependent and scale-dependent (Cunha et al., 2012; Lobligeois et al., 2014; Mandapaka et al., 2009; Seo et al., 2012; Tetzlaff and Uhlenbrook, 2005; Viglione et al., 2010). Even though there was no unified answer as to how each facet of rainfall spatial-temporal variability impacts streamflow (Andrés-Doménech et al., 2015; Nicótina et al., 2008), detailed knowledge of spatial rainfall was found to reduce the estimation error of highly resolved hydrological models (Müller-Thomy et al., 2018). In general, for medium-sized catchments (with areas of a few hundred square kilometres), high spatial (~1 km^2) and temporal (1 h) resolution rainfall data are perceived to be necessary in extreme flow estimation (Müller-Thomy et al., 2018; Tetzlaff and Uhlenbrook, 2005).

In order to estimate long-term flood risk, many rainfall models have been developed to represent rainfall information at such scales because of lack of observations. Then, the simulated

rainfall fields can be fed into hydrological models to estimate catchment response either in the present climate or in future climate scenarios (Peleg et al., 2017a; Winter et al., 2019). An approach would involve making direct use of physically based weather and climate models (Kay et al., 2009; Prudhomme et al., 2002). Even though physically based, those models, particularly at coarser scales (Global circulation models / Region circulation models), are known to suffer from biases (Sillmann et al., 2013). Climate models' ability to generate realistic precipitation was recently improved by representing processes at fine spatial and temporal scales (i.e. Convection Permitting Models (CPMs)). This enables detailed simulation at local scales which can be used for flood impact studies without the need for downscaling (Chen et al., 2021; Kendon et al., 2012; Prein et al., 2015). However, for most hydrological applications, the huge computational requirements of CPMs are still prohibitive. The uncertainties related to the natural variability, model uncertainty and parameter uncertainty also limit their direct use (Kay et al., 2015). As opposed to climate models, stochastic rainfall models adopt a conceptually simpler statistical framework to generate rainfall time series or fields. The framework makes rainfall generation computationally efficient and therefore able to capture the full variability of climate systems. Because of those features, stochastic models are perceived to be a suitable tool for hydrological applications, particularly when analysis of variability and extremes is essential (Fatichi et al., 2016).

Early stochastic modelling attempts focused on reproducing hourly rainfall at a single site, neglecting spatial variability (Cameron et al., 2000; Cowpertwait, 2004; Onof and Wheater, 1994; Waymire and Gupta, 1993). In the last few decades, more advanced measurement technologies such as satellite and dual polarization Doppler radars have enabled us to better understand the spatial structure of rainfall. Such knowledge allowed for the development of

detailed spatial-temporal stochastic rainfall models at hourly or sub-hourly resolution (Bell, 1987; Cowpertwait, 1995; Gires et al., 2012; McRobie et al., 2013; Over and Gupta, 1996; Paschalis et al., 2013; Peleg et al., 2017b; Wheater et al., 2005), to name but a few.

Among those, models based on point processes are one of the widely used categories in hydrological applications. One advantage of point process models is the availability of analytical expressions for key statistics of modelled rainfall, including moment estimates up to the third-order moment, probability of dry period, autocorrelation and spatial correlation (Cowpertwait, 1994; Leonard et al., 2008; Northrop, 1998; Onof and Wang, 2020). These key statistics can be directly included in the model calibration. Another advantage lies in the possibility of continuous rainfall simulation, which potentially overcomes the drawback of event-based simulation in long-term flood risk analysis (Verhoest et al., 2010). Point process-based models can be divided into (1) models based on Poisson-cluster processes, namely the Bartlett-Lewis and Neyman-Scott point processes (Burton et al., 2008; McRobie et al., 2013), which differ in terms of their clustering mechanism (Onof et al., 2000), (2) models based on Cox processes (Ramesh et al., 2013). Despite having many promising features, typical problems of many published spatial-temporal models based on point processes are the lack of storm movement, the lack of statistical dependence between rainfall properties (intensity and duration) and the underestimation of rainfall extremes at fine space and time scales (Paschalis et al., 2013). Northrop (1998) introduced storm movement by increasing the detail of rainfall structure at the event scale, but generalizations to continuous-time rainfall models are not straightforward. By embedding this model within a renewal process generating wet and dry spells, a non-parsimonious continuous-time model was obtained whose model calibration was very data demanding (Wheater et al., 2006). There were also attempts to reduce the underestimation of extremes by including some

dependency between rainfall properties (Evin and Favre, 2008; Kaczmarska et al., 2014; Park et al., 2019; Paschalis et al., 2014b). However, since they focused predominantly on single site models; these improvements cannot readily be applied to spatial-temporal versions.

To date, the space-time Neyman-Scott rainfall model has been extensively used for flood estimation (Brath et al., 2006; Camici et al., 2014; Moretti and Montanari, 2008; Rulli and Rosso, 2002; Sordo-Ward et al., 2016) particularly when a continuous hydrological simulation is preferred. This type of model was used as the basis for the RainSim modelling tool (Burton et al., 2008), initially developed by Cowpertwait (1995), with further improvements in recent years (Burton et al., 2010; Cowpertwait, 2010; Leonard et al., 2008). The model was calibrated using long-term rainfall observations, commonly rain gauge measurements. Most of the previous research applied this type of model (Burton et al., 2010; Cowpertwait et al., 2002; Leonard et al., 2008; Segond and Onof, 2009) to estimate streamflow either on ungauged basins or areas without long-term flow data. The validation of the rainfall model in terms of the resulting streamflow was limited by the data available at these study areas. Although the simplification of rainfall structure in this model has been recognized, up to now, little attention has been paid to the quantification of how the simplifying rainfall structure assumptions propagate errors to runoff estimates (Felder and Weingartner, 2016; Verhoest et al., 2010).

This study aims to investigate to what extent the estimation biases in the space-time rainfall model based on point processes propagate to the estimated streamflow. We set up a numerical experiment to quantify such biases at two medium-sized catchments located in the UK. A fully distributed hydrological model, one of the most advanced point process models in the literature, a dense network of hourly rain gauges and one of the last generation rainfall radar data sets in the UK are applied to the study area. Using those tools, we quantify the estimation

biases of the generated hourly space-time rainfall and their effect on catchment scale dynamics, with an emphasis on high flows.

2 Study sites and Data

2.1 Site Description

The numerical experiment proposed was carried out for two rural catchments (Fig. 1) located in the Anglian river basin (south-east of the UK), namely Stour and Welland. Characterized by a temperate oceanic climate, the south-east has the greatest density of mesoscale convective storms over the UK (Gray and Marshall, 1998; Lewis and Gray, 2010). The area (Anglian region) receives annual rainfall around 700 mm (Met Office, 2016). The precipitation is spatially uniform with negligible orographic effects (Neal and Phillips, 2009). As a typical low-lying part of the country, despite the low rainfall totals, this area experiences large fluvial flooding events resulting in significant flood damages (DEFRA, 2016a, Table 7.1). For example, the total economic damages of the winter floods of 2013 to 2014 is estimated to be 1.3 billion pounds in England and Wales (Environment Agency, 2016).

The Stour catchment at the Stratford cross section (844 km^2) is located at low altitude (5.6-127.6 m), running from west to east along 75.6 km of the mainstream. Land cover consists mainly of arable land (75.37%) and grassland (13.94%) (NRFA, 2019a) (See Figure S1). The geology is characterized by chalk underlying clay soils, fluvial sands or gravels (Anstead and Tovey, 2017). The main flood risk is from river flooding due to soil saturation excess (DEFRA, 2016b, p. 48), while incidents of groundwater flooding are limited (DEFRA, 2009a).

The Welland catchment at the Tallington cross section (717 km^2), compared with the Stour catchment, has a steeper topography (7.6-229.3 m) (Fig. 1.b). The land cover (see Figure S1) is

mainly arable for crop production (47.21%) and grassland (34.45%). The underlying geology is nonporous clay, with a high runoff coefficient (DEFRA, 2009b). Similarly, river flooding is the main risk in this catchment (DEFRA, 2016b, p. 133).

2.2 Rainfall Data

In this study both rain gauge and radar data were used. Gauge measurements with 1-hour resolution were obtained from 54 stations (Fig. 1.a) equipped with tipping bucket rain gauges with further quality controls (Blenkinsop et al., 2017, Table 1). The rain gauge data has depth resolution of 0.2 mm and covers the period between 2005 and 2016.

Radar data were used to provide the spatial information about the rainfall, obtained from the operational C-band network of the UK Met Office (Met Office, 2003). In this study the quality-controlled post-processed radar composite at a spatial resolution of 1×1 km in space and 1 h in time (aggregated from 5 min data) was used, for the period 2007-2015. We further corrected the radar data using mean field bias (MFB) adjustment (Biggs and Atkinson, 2011; Ochoa- Rodriguez et al., 2019) to mitigate biases due to beam blocking and ground clutter. In the MFB adjustment, daily gridded estimates from the CEH-GEAR rainfall product, available at the same 1 km × 1 km resolution (Tanguy et al., 2019) were used for the estimation of the correction factors.

2.3 Site data

Catchment data used for setting up the hydrological model include topography, land use, soil textural properties and geology. The topography was extracted from OS Terrain 50 (Ordnance Survey, 2018) digital terrain model and regridded to 200 m × 200 m resolution. The soil textural properties (fraction of sand, clay, silt and organic matter in the first 500 mm depth)

were obtained from SoilGrids (Hengl, 2018a, 2018b; Hengl and Wheeler, 2018). These soil properties were then converted to spatially distributed soil hydraulic properties (see Figure S2) using the Pedotransfer functions of Saxton & Rawls (2006).

Potential evapotranspiration was taken from the 1 km × 1 km gridded product (CHESS-PE) provided by the UK Centre for Ecology and Hydrology (Robinson et al., 2016). This product contains potential evapotranspiration from 1961-2015 at a daily scale, calculated using the Penman-Monteith equation (Monteith, 1965) from the Food and Agriculture Organization of the United Nations (FAO). For the calibration of the hydrological model, gauged daily river flows at two upstream stations were used, retrieved from the UK National River Flow Archive (NRFA).

3 Methods

3.1 Stochastic Rainfall Generator

One of the most advanced point process models (Cowpertwait, 2010) was applied to the study region (Fig. 1.a) which covers the two river catchments. Compared with the earlier and more widely used version of the Neyman-Scott based space-time model (Burton et al., 2008; Cowpertwait et al., 2002), the spatial representation of this version has been found to improve on it (Leonard et al., 2008). The model is capable of representing most key properties of point rainfall and spatial correlation at both hourly and daily resolution, and with a parsimonious structure (Cowpertwait, 2010; Cowpertwait et al., 2013). The most attractive feature of the model is that it has available analytical expressions for the moment estimates of the marginal distribution of the point rainfall depth, its temporal autocorrelation function, the probability of rainfall across temporal scales, as well as the cross-correlation of rainfall depths at any temporal scale. These expressions are used for model calibration. Simulated ensembles are continuous in

191 space and time, but for this study we aggregated them at a 1 km^2 spatial resolution and 1-hour
192 temporal resolution.

193 ***Model Structure based on Point Process***

194 The stochastic tool is a Neyman-Scott Point process rainfall model (NS(s-t)). The model
195 generates rainfall in two steps: First it generates storm arrivals and then generates the inner-storm
196 cells. The model assumes that storms are independent, i.e. arrive in space and time according to a
197 spatial-temporal Poisson process with a rate ζ_s (per unit area per unit time). The storm envelope
198 defines the spatial extent within which the rainfall can occur (Fig. 2). The envelope has an
199 exponentially distributed radius with parameter $\gamma_s(km^{-1})$. Rain cells appear after the storm
200 arrival time according to an exponentially distributed delay; this exponential distribution has
201 parameter β (unit: h^{-1}). The number of rain cells C associated with the storm follows a Poisson
202 distribution with a parameter ν $(-)$.

203 Rain cells are defined as discs over which the rainfall intensity is constant in space and
204 time during the lifetime of the cell. The cell radius is exponentially distributed with parameter
205 $\gamma_c(km^{-1})$. Cells are characterized by their lifetime, intensity and radius. These properties follow
206 mutually independent exponential distributions, with parameters $\eta(h^{-1})$, $\xi(h \cdot mm^{-1})$ and
207 $\gamma_c(km^{-1})$ respectively. Under the model, the rainfall at a particular location and a particular time
208 is the superposed intensity of all cells covering that point at that moment.

209 In order to capture the characteristics and the combined effect from different types of
210 rainfall systems, a governing parameter z is included in the model. The parameters mentioned
211 above (ξ, ν) are adjusted to be functions of the additional random variable z, which is associated
212 with the storm characteristics (see Text S1). The value of z is continuously distributed according
213 to a distribution with probability density function f_z.

One advantage of this version of the model is that a defined storm extent is included in order to achieve greater physical realism over a large area (Leonard et al., 2008). A storm envelope (defined by a randomized storm radius) is taken as a constraint so that only the part of a cell inside this envelope contributes to the storm rainfall (Fig. 2). Hence the target region of interest might be partially covered by the generated storms, potentially alleviating the poor behaviour of the Neyman-Scott model without this constraint into properly capturing the fraction of wet area in the catchment (Paschalis et al., 2013).

Spatial heterogeneity is included in the model by adding a scale parameter φ_{P} to adjust ξ (the parameter governing the cell intensity) at each site. The added scale parameter enables the model to generate a spatially varying pattern of mean rainfall intensity while keeping other dimensionless moment estimates spatially uniform. All other model parameters are valid for the whole area, and the calibration of these parameters can be undertaken for the whole dataset. For the model calibration in this study, the scale parameters were obtained exclusively from the rain gauge data, whereas to generate the stochastic ensembles the GEAR product was used.

Stochastic Model Calibration

The model was calibrated by minimizing the objective function formed with the moment estimates of the observed and the modelled rainfall series. Statistical properties of modelled rainfall time series (at a certain aggregation level h) include the mean intensity $\mu(h)$, the coefficient of variation $\upsilon(h)$, coefficient of skewness $\kappa(h)$, lag 1 autocorrelation $\rho(0,1,h)$, cross-correlation $\rho(d,0,h)$ and probability of dry period $\varphi(\mathrm{h})$, where d is the distance between two sites (see analytical expressions in Text S2). Following the previous study by Cowpertwait (2010), the Poisson parameter ν is a function of variable z (z is related to rainfall types): $\nu(z) =$

$(1-z)\nu_0 + z\nu_1$, where ν_0 and ν_1 are two model parameters. Model parameters to calibrate are $\{\lambda, \nu_0, \nu_1, \beta, \eta, \gamma_s, \gamma_c\}$ (for each calendar month).

The Generalized Method of Moments (GMM) is applied to estimate the model parameters $\boldsymbol{\theta}$. $\boldsymbol{\theta}$ is estimated via the minimization of

$$\underset{\boldsymbol{\theta}}{argmin}\left(\sum_{i=1}^{k}\sum_{h\in H}\sum_{s=1}^{m}\left(w_{i,h,s}\left[T_{i,h,s}-\tau_{i,h}(\boldsymbol{\theta})\right]^2\right)\right) \quad (1)$$

where h is the time scale of aggregation, s the site, $T_{i,h,s}$ the observed estimate of statistical property number i at scale h and site s; $H = \{1,6,24\ hour\}$; $\tau_{i,h}(\boldsymbol{\theta})$ the modelled estimate of the same for any site (the model is spatially stationary) and $w_{i,h,s}$ is the weighting factor assigned to this statistical property.

In the model, $\{\mu(1), \upsilon(h), \kappa(h), \rho(0,1,h), \rho(d,0,h), \varphi(24) : h = 1,6,24\ hour\}$ were used in the calibration. The weighting factors are set to the inverse of the variances of the statistics (Kaczmarska et al., 2014). Notably, in the spatial model we use, the $w_{i,h,s}$ and $T_{i,h,s}$ were computed for each site separately instead of pooling all sites together. This enables the sites having a larger variability of statistics (expected to have higher uncertainty) to be assigned a lower weight in calibration.

The calibration procedure otherwise follows that in Cowpertwait (2013) and is based on the use of statistics of hourly rain gauge data. Within it, the probability distributions of the random rainfall type z and the corresponding other dependent parameters is predefined following the settings in previous research (Cowpertwait, 2010). The calibration steps are described below.

(a) The optimal set of temporal parameters θ for each calendar month is estimated. Here, $\theta = (\lambda, \nu_0, \nu_1, \beta, \eta)'$, T $= \{\upsilon(h), \kappa(h), \rho(0,1,h), \varphi(h) : h = 1,6,24\ hour\}$. Firstly, a minimisation based on a random 'Multi-start' method is undertaken by using Sequential

Quadratic Programming. The minimisation is evaluated with 20 initial estimates, so as to avoid local minima. The optimal parameter set obtained from this step is denoted as θ^o.

Then, in order to obtain a smooth variation in monthly parameters, for each month the parameter set θ^o is used for deriving a final set of parameters θ. The final parameter sets θ is obtained by minimizing the equation (1) with an updated initial parameter guess (equal to a 3-month moving average of θ^o).

(b) After obtaining the final temporal parameter set $\{\lambda, \nu_0, \nu_1, \beta, \eta\}$, space-related parameters γ_s and γ_c are further optimized by minimizing the sum of squares (Cowpertwait et al., 2013, Equation 1) using a genetic algorithm to avoid a local optimum. This therefore yields a complete parameter set $\{\lambda, \nu_0, \nu_1, \beta, \eta, \gamma_s, \gamma_c\}$ for each calendar month (see the 7×12 parameters in Table S1).

$$\underset{\{\gamma_s,\gamma_c\}}{\operatorname{argmin}} \left\{ \sum_{h\in H} \sum_{d\in \mathcal{D}} \left(1 - \frac{\hat{\rho}(d,0,h)}{\rho(d,0,h)}\right)^2 + \left(1 - \frac{\rho(d,0,h)}{\hat{\rho}(d,0,h)}\right)^2 \right\} \quad (2)$$

where $\mathcal{D}$ is the set of distances for all pairs of gauged sites.

(c) In the final step, the scale parameters $\{\varphi_{\mathrm{P}}\}$ (unit: mm) for calendar months are estimated (Cowpertwait, 2010). For each location p, the model parameters which are used for rainfall generation are $\{\lambda, \nu_0, \nu_1, \beta, \eta, \gamma_s, \gamma_c, \varphi_p\}$.

$$\hat{\varphi}_p = \frac{6\hat{\mu}_p(1)\hat{\eta}}{\hat{\lambda}(\hat{\nu}_0 + \hat{\nu}_1)} \quad (3)$$

where $\hat{\mu}_p(1)$ is the 1h sample mean for site p in the corresponding calendar month.

3.2 Hydrological model

A calibrated fully distributed hydrological model was used to simulate rainfall-runoff processes in the catchments. In this section, we provide some description of the model and background of its calibration.

The model is the WATET model (Remondi et al., 2018) without explicit consideration of the pollutant transport as this is not relevant for this study. Briefly, the model solves hydrological fluxes on a regular grid. Soil water is solved using a simplified soil water transport model for every grid cell for computational efficiency. This model is similar to the grid-to-grid model by Bell (2007). Similarly, surface water routing and lateral soil water flow are estimated by using a kinematic wave approximation.

In order to provide a more accurate representation of topographic features, the spatial resolution of the DEM was chosen to be 200 m × 200 m. Infiltration and evapotranspiration were solved at an hourly time step. Surface water was routed by using an adaptive time-step which could be as small as a few seconds, based on the Courant–Friedrichs–Lewy condition (Courant et al., 1928). Evapotranspiration was estimated as a product of potential evapo-transpiration (PET) and a water stress factor β was set equal to the average effective soil moisture of the 45 cm of soil (Porporato et al., 2001). The soil hydraulic properties were estimated using a Pedotransfer function (Saxton and Rawls, 2006) based on soil textural properties we obtained. Groundwater flow was represented as a storage-discharge relationship $\mathrm{Q}_{gw} = aS_{gw}^{b}$ (Benettin et al., 2015), where a, b are two empirical coefficients. Urban runoff and contributions of man-made drainage networks were neglected in this study.

Aside from the available spatially distributed catchment information (section 2.3), there were several other parameters required to set up the hydrological model, including the hydraulic

conductivity anisotropy ratio, the root zone depth, the maximum groundwater storage and the exponent in the storage-discharge function. Model calibration was thereby carried out before the numerical experiment to define all the parameters of this hydrological model. These were estimated (Table 1) by maximizing the Nash-Sutcliffe efficiency (NSE) (Nash and Sutcliffe, 1970) of daily streamflow at two gauging stations (Brett at Cockfield and Bumpstead Brook at Broad Green). In model calibration, observed rainfall using the combined radar/rain gauge data was taken as rainfall input. These two stations were chosen because both are part of the UK Benchmark Network (UKBN), which is expected to be 'near-natural' and can be considered as reasonably free from human disturbances (Harrigan et al., 2018; NRFA, 2019b). Daily streamflow measurements between 2008 and 2015 were used in calibration (see a full hydrograph in Fig. 3, zoom-in hydrographs and hyetographs in Figure S3), while the year 2007 was used for the model spin up. The NSE values for the two stations were 0.68 and 0.60 for daily flows. Note, both stations are in the Stour catchment, and there are no gauged stations belonging to UKBN in the Welland catchment. At Welland, we checked that the parameters enable the model behaviour to broadly replicate the Welland catchment by selecting an upstream station (Gwash South Arm at Manton), thus largely excluding the effect of built infrastructure. The NSE value was 0.54 for daily flow at Manton station. Model skill to replicate the observed streamflow is clearly not optimal (i.e. NSE=1) for the catchments (Ritter and Muñoz-Carpena, 2013). This is due to the simplifications introduced by the hydrological model and uncertainty related to the observed catchment information. However, for the purpose of this paper, this is not an issue. For this numerical experiment we considered the modelled runoff using observed data as our *reference runoff*. All comparisons of runoff properties were made against this reference case. This means that the catchments we used to test the rainfall models are not the real ones, but

virtual catchments defined as those for which the model is perfect. A perfect replication of the real catchment runoffs is therefore not required in this study.

3.3 Numerical Experiments

The evaluation of the rainfall generator includes two parts: analysis of the synthetic rainfall field and analysis of its resulting catchment response. For the study region, we generated synthetic hourly rainfall spatial fields after calibrating the rainfall model by using 12 years of hourly rain gauge data (Fig. 2.a). Gridded scale parameters $\{\varphi_P\}$ at 1 km^2 resolution were computed by interpolating the scale parameters at the 54 sites, given the gridded average rainfall amount from the GEAR dataset (Text S3). Therefore, the spatial-temporal rainfall model exactly preserves the observed spatial distribution of long-term annual rainfall amounts in the GEAR dataset through the variation of scale parameters (Figure S4). 100 simulation replicates generated from the rainfall generator were used to validate rainfall statistics. Each replicate represents 12 years of data, i.e., the same length as the sample data.

Regarding the hydrological simulations, the calibrated hydrological model was used for the 2007-2015 period (9 years). To evaluate how the errors of the stochastic rainfall model propagate through the catchment response, the modelled catchment response was compared with the reference runoff. The resolution of all rainfall inputs is 1 hour in time and 1 km × 1 km in space. For the modelled catchment response, 20 stochastic ensembles were used to represent the stochastic variability (Figure S5, S6).

3.4 Statistical Analyses

Point rainfall statistics

We compared the mean, the coefficient of variation (CV), the coefficient of skewness (SKEW) and the lag one autocorrelation of rainfall depths at each site (ACorr), the cross-correlation of rainfall depths between sites (CCorr) and the probability of dry period at each site (PD) between modelled and observed rainfall. Daily and hourly temporal scales levels were chosen. These statistics were included in the model calibration of NS(s-t) and have been commonly used to validate point process stochastic models (Cowpertwait et al., 2013). The overall performance of these key descriptors was represented by the average of the relative bias between the fitted value and the sample value.

Extreme Value Analysis

Extremes (annual maxima) of point rainfall were evaluated, at both hourly and daily aggregation levels. We evaluated key properties of the point extremes over the study area. For the kth simulation of the set of 100 12-year-long simulations, the ranked annual maximum in the ith year at site s is denoted as $y_{k,i,s}$. The annual maxima are assumed sorted from largest to smallest, so that $y_{k,i,s} \geq y_{k,i+1,s}$. Let $q_{\alpha,i,k}$ be αth quantiles for the year i and the simulation k over all sites of $y_{k,i,s}$. $m_{\alpha,i}$ is the median over all simulations k of $q_{\alpha,i,k}$. We calculated $m_{\alpha,i}$ for $\alpha = 0.1, 0.25, 0.5, 0.75, 0.9$, and plotted these on the usual Gumbel plot. That is: the horizontal axis is the Gumbel reduced variate $y(i) = -ln(-ln(1 - 1/T))$, where $T = (N + 0.12)/(i - 0.44)$ following the Gringorten formula and $N = 12$; the vertical axis is the value of $m_{\alpha,i}$. For the observational data, k = 1.

Areal statistics

To test if the model captures well the areal statistics, we used Areal Reduction Factors (ARFs), the wet area ratio and the areal mean precipitation intensity to evaluate simulated rain fields, at the hourly scale. The Areal Reduction Factor was estimated by using the fixed-area

363 method (Svensson and Jones, 2010). The method calculates a ratio of the point-measurement
364 when the point rainfall reaches the annual maximum to the point-measurement when a certain
365 areal rainfall reaches the annual maximum. Multiple return periods were not considered here,
366 which is one limitation of the fixed-area method (Bell, 1976). In order to reduce the effect of this
367 limitation, the same length of data was therefore applied to compute each ARF. We compared
368 the ARFs computed from the observation and synthetic rain fields, for durations of 1, 2, 6 and 24
369 hours. A larger value of ARF indicates a higher similarity between the point and the areal rain
370 intensity.

371 The wet area ratio is the fraction of wet area in the simulation domain, where grid squares
372 having hourly rainfall depth larger than 0.2 mm are defined as 'wet' grids (1 km resolution). The
373 areal mean precipitation intensity was computed for each snapshot of the rainfall field (717 km^2)
374 at several time scales (1 hour, 6 hours and daily). The wet area ratio is also considered as a key
375 characteristic of the rainfall structure in determining the runoff in the catchment study. The two
376 variables were computed, and their probability distributions were used to compare the simulated
377 rainfall with the observed.

378 ***Runoff statistics***

379 Flow duration curves (FDCs) and flood frequency curves (FFCs) (Lamb et al., 2010) were
380 used to evaluate the statistics of the resulting runoff driven by different rainfall forcings. Both
381 curves were derived using the continuously simulated flow data (at catchment outlets) of the
382 hydrological model. FDCs were used to assess the variation of flow series. Curves for both the
383 low flow period (June to August) and the high flow period (December to February) were plotted.
384 FFCs were used to assess the simulated extreme streamflow, reflecting the potential risk of river
385 flooding. Flood frequency curves were plotted on a seasonal basis. A Gumbel distribution was

assumed to fit the FFCs, the confidence intervals of which were estimated by employing a parametric bootstrap method (Coles, 2013).

Spatial pattern of soil moisture

To provide an insight into runoff generation in the catchment, we used the saturated fraction of soil (Paschalis et al., 2014a) to describe the spatial distribution of the upper layer soil moisture throughout the long-term hydrological simulation. Saturated fraction is the fraction of area where the soil is close to saturation (having an effective soil saturation of the upper soil layer S_e > 0.95). As runoff generation in our case is almost exclusively saturation excess (not shown here), the fraction represents the catchment area contributing to river discharge. The maximum saturated fraction was extracted for each identified storm, to prevent double counting. Storms were individuated by the condition that inter-storm time be a dry period (rainfall depth less than 0.2mm) of at least 12 hours. Conditioned on areal mean intensity within the event, we compared the saturated fraction of different rainfall forcings and in different seasons.

4 Results and Discussions

4.1 Stochastic model performance

The fitting performance of the rainfall model in terms of temporal-related properties included in model calibration was examined, at 1h, 6h and 24h aggregation level (Fig. 4.a-4.e). The stochastic model is able to reproduce the long-term annual mean precipitation (with a relative bias less than 0.76%) and the inter-annual variability (Fig. 4.e).

At the hourly scale, the calibrated model reproduced the coefficient of variation (CV), the coefficient of skewness (SKEW), and the autocorrelation lag-1 (lag-1 ACorr) (month-average relative error is 0.64%-3.37%) (Table 2). The lowest skill is found in the reproduction of SKEW,

specifically during the summer season (Fig. 4.c). This low skill can be attributed to the calibration weights w_i (equation 1): a lower weight is assigned to this statistic due to its high variability.

At the daily scale, the reproduction of rainfall statistical properties is prone to slight biases (relative error is 2.82-18.89%), with SKEW being the best and the lag-1 ACorr the worst reproduced statistic (Table 2). Even though the model performs well in capturing autocorrelations for larger lags (Figure S7), a consistent underestimation of daily lag-1 autocorrelation is observed during the winter season (Fig. 4.b). This implies the model's weakness in capturing prolonged rainfall events, often occurring during winter.

The probability of zero rainfall hours is not used in model calibration but examined in the validation (Fig. 4.d). We consider all hours with rainfall intensity < 0.2mm/h as dry. The average error of this statistic is in general small with its worst performance during September.

The spatial correlation of synthetic series at the hourly scale for two months, January and June, is representative of winter stratiform and summer convective events and is therefore used for comparison (Fig. 4.f, 4.g). The seasonal pattern of cross-correlations is well captured by the stochastic model. During the winter season, when stratiform systems with large spatial extent commonly occur the model captures well the spatial correlation. However, during summer, the model overestimates the spatial correlation for distances smaller than 50 km (Fig. 4.g), suggesting a low skill in capturing the localized features of convective summer storms. Another useful metric to represent the realism of spatial rainfall fields, the 'continuity ratio' (Wilks, 1998), was also evaluated in the Supplement to this paper (see Text S4 for definition and results). results are consistent with Fig. 4.f, 4.g.

Point-scale precipitation extremes were analysed on a seasonal basis (Fig. 5). The extremes produced by the NS(s-t) model show an overall good agreement with the observed extremes at return periods of up to 20 years. A slight underestimation is found, mainly in summer (JJA), when the model produces a lower hourly extreme (2.9mm/h lower for 20-year return levels). Underestimation is a familiar problem in temporal modelling of rainfall with Poisson-cluster models (Paschalis et al., 2014b; Verhoest et al., 2010) and is closely connected to the relatively short tail of the distribution of rainfall cell intensity; thicker tail distributions could be used, but this typically negatively impacts other statistics (Kaczmarska et al., 2014). Short-but-intense rainfall events are supposed to have greater peak intensity and higher hourly extremes, hence the more significant discrepancy in summer seasons. For return levels larger than 8 years, simulated hourly extremes across sites are generally smaller than the observed.

Because of the computational time required, the analysis of areal statistics is based on 20 generated rainfall ensembles gridded at a 1 km^2 resolution over the study region (19000 km^2), i.e. at a resolution identical to that of the radar observations. The estimated error of ARFs (Fig. 6.a) at a daily scale is a mere 2% for areas smaller than 1000 km^2. But a larger overestimation of the ARF is observed at sub-daily scales with the worst performance being at the hourly scale (relative bias is 23% for areas of 400 km^2). The increasing bias of the ARFs with larger area size highlights the fact that the NS(s-t) model overestimates the dependency between the point rainfall amount and the areal rainfall amount at the same time. The overestimation is not surprising because observed rainfall cells have a distinct spatial feature from the modelled cell structure, such as peak intensities and variable rainfall intensity (Hardenberg et al., 2003). In the model, at a given time step, rain cells are assumed to have constant rainfall intensity in space. The resulting correlation between the areal rain and the point rain derived from the NS(s-t)

model is higher than for the observed rain, where the Pearson correlation is 0.84 and 0.78, respectively. Higher ARFs are therefore estimated by the NS(s-t) due to the stronger spatial dependence. The overestimation of ARFs is more prominent during the summer season (Figure S8). This can be explained by the models' low skill in simulating short-lived intense convective summer rainfall (Breinl et al., 2020). The overestimation is also consistent with the overestimation of spatial correlations during summer events (Fig. 4.f, 4.g).

Although the point-scale precipitation intensity is well preserved by the rainfall model (Figure S9), the computed areal mean precipitation intensity (Fig. 6.b) shows a pattern consistent with the computed ARFs as the bias is more pronounced at finer scales. Synthetic hourly extremes for an exceedance probability < 0.01% are 8.0 -13.5 mm/h, 1.6 - 7.1 mm/h larger than the observed intensity (6.4 mm/h). In terms of the daily extremes, at the same exceedance probability, the range of synthetic daily areal mean precipitation intensity (22.5 - 46.9 mm/day) is consistent with the observed value (28.9 mm/day). The bias in the mean areal intensity we reported here is smaller than the bias reported in a previous work (Paschalis et al., 2013): this reduction follows from the improved representation of spatial correlation in the model (Leonard et al., 2008).

This bias in the mean areal intensity can be explained by the modelled cell structure. Firstly, the model does not correctly preserve the feature of those localized, short but intense rain cells. Because of the assumed independency, those very intense cells could cover a larger area and last for a longer duration in the modelled than in the observed data. Secondly, compared to the bell-shaped rainfall cell in observations, the constant intensity throughout a modelled cell leads to a smaller coverage of wet area but a larger amount of rainfall within the wet area, thereby yielding a higher tail value. When it comes to the daily scale which is larger than the

typical duration of summer storms, the overestimation is weaker and the influence of the misrepresented spatial extent of cells is expected to be largely eliminated.

Other seasons follow a similar trend as Fig. 6.b except spring (MAM), which shows an underestimation at the daily scale. The lower daily areal extremes in MAM can be explained by the underestimation of the coefficient of variation in March and May (Fig. 4.a) and the daily-scale coefficient of skewness in April (Fig. 4.c).

When comparing the spatial extent of wet spells (Fig. 6.c), the wet area ratio is underestimated by 16.31% - 31.77% on average, for both localized storms with smaller cell sizes and wider stratiform events. This is mainly due to the model not representing the small-scale spatial storm structure and the time evolution within a rain cell. The modelled rain cells are static and cylindrical, which is a simplification of typical bell-shape moving cells shown in radar observation (Hardenberg et al., 2003). Under the simplification, the superposed spatial extent of all rain cells occurring over an area at a certain duration is overall narrower than the observed area. In order to form a cylindrical shape as the model assumes, the edges having a low rain rate are therefore moved closer to the cell centre, which has the effect of lowering the modelled wet area ratio.

It is true that the performance of a model is largely determined by model calibration. Current model calibration is based on the Generalized Method of Moments, in which the weighting of each property is set to be the inverse of variance. The calibration gives a robust approximate to the optimal parameters (Jesus and Chandler, 2011). Additional procedures such as Depth-Duration-Frequency (DDF) analysis could be introduced to adjust the calibrated model parameters through a trial-and-error method, which is implemented for a single-site Neyman-Scott model (Moretti and Montanari, 2008). However, the adjustment criteria are subjective, and

those fitted key statistics would change after the manual adjustment. Also, if it is applied to the space-time model, the resulting computational burden would be challenging. For each potential parameter set, a long-term space-time simulation (20 years or even longer) would be required to obtain the DDF curves. Additionally, the simulated DDF will be 'optimized' at the expense of increasing the estimation bias of some other key statistics (those used in the model calibration) at a point scale. Even though point statistics such as the autocorrelation could be better represented, the spatial structure of rain cells and the wet area ratio at a catchment scale are unlikely to reduce to a large extent.

4.2 Bias propagation from rainfall to runoff

By using the calibrated hydrological model, simulated runoff time series are obtained for both observed rainfall input and each realization of stochastic rainfall (Figure S10). The sensitivity of hourly Flood Duration Curves (FDCs) to rainfall forcing scenarios is then compared for the catchment outlets, during both low flow (Summer, JJA) and high flow seasons (Winter, DJF). In the flow duration analysis (Fig. 7), the FDC for the reference runoff is within the range of variability of the simulations that use stochastic rainfall as input. For the median streamflow (Q50) during winter, NS(s-t) modelled rainfall reproduces the runoff in both catchments, with a relative bias less than 6.70% (Fig. 7.b, 7.d). During summer, NS(s-t) produces a Q50 streamflow close to the reference runoff, with the relative bias between 4.96% and 32.5% (Fig. 7.a, 7.c). FDCs of hourly streamflow give a similar pattern (not shown here). We note that in the Stour catchment the simulated summer flow is generally low (~0.1 m^3/s), both for the reference runoff and the runoff generated using the NS(s-t) forcing. The low value is associated with the summer drought in the catchment and the omission of crop irrigation in the hydrological simulation.

In light of this, we analysed the flood frequency curves (FFCs) on a seasonal basis whereby the analysis for summer was solely based on the Welland catchment (Fig. 8.a, 8.b). At an aggregated daily scale (Fig. 8.a), the ensemble range of the NS(s-t) produced runoff covers the 95% confidence interval of the reference runoff. On average, the NS(s-t) results in a 2.9 m^3/s higher peak discharge for a 10-year return level, where the relative bias is 16.9%. It suggests that the simplified spatial organization and neglected movement of single cells assumed in the model do not largely affect the resulting peak discharge at the daily scale. This behaviour is likely due to the filtering role of the catchment, where the effect of spatial-temporal variability of rainfall on runoff is smoothed over the catchment area and alleviated by the concentration time (Andrés-Doménech et al., 2015). Therefore, the daily peak discharge is well preserved by the NS(s-t) model with only a slight overestimation. This overestimation is consistent with the slightly overestimated areal mean precipitation extremes at a daily scale (Fig. 6.b) where the estimation bias is not significantly magnified in the rainfall-runoff transformation.

At a finer scale (e.g., hourly), a different pattern of FFCs is observed during summer (JJA) (Fig. 8.b). The hourly discharge of a 10-year return level (averaged over 20 ensemble simulations) produced by the NS(s-t) model (63.58 m^3/s) is 163.5% higher than the reference discharge (24.13 m^3/s). The overestimation implies that the error in the representation of the hourly areal extremes (Fig. 6.b) is not filtered out by the rainfall-runoff transformation. Instead, the misrepresentation is amplified, leading to a greater peak discharge than the theoretical one. At the hourly scale, the spatial variability of summer rainfall is expected to play a vital role in modulating peak discharge, aside from the inter-dependency of rainfall properties.

In terms of the FFCs during the winter season (DJF), the ensemble range of simulated discharge of the stochastic forcing largely overlaps with the 95% confidence interval of reference

curve (Fig. 8.c-8.f). At a daily aggregation level, the relative bias of the 10-year flood (ensemble average) is 0.36%-9.23% (Fig. 8.c, 8.d). At an hourly scale, the relative bias at the same return level is 5.80%-25.96% (Fig. 8.e, 8.f). Although the stochastic model yields a greater value of areal rainfall extremes, at the Welland catchment, the winter peak discharge turns out to be slightly underestimated. The estimated result might be a joint effect of a higher areal extreme but shorter-lived rainfall event produced by the stochastic forcing, compared with the flood-inducing rainfall events. Besides the fact that the fitted model underestimates the observed daily autocorrelation, in the UK extreme winter flooding is largely associated with atmospheric rivers (ARs) (Lavers et al., 2011; Ralph et al., 2006). The accompanying large amount of water vapour as well as the strong winds further strengthen the dependency between event duration and intensity in this type of extreme event. Simulation of this dependence structure is expected to be crucial for the purpose of hydrological design (Callau Poduje and Haberlandt, 2017), while these properties are independent in the cells of the rainfall model.

It is worth mentioning that the fitting methods used for the extreme value analysis affect to some extent the magnitude of fitted maxima, all the more so as the sample is only 9 years long. Several fitting methods have been tested, including generalized maximum likelihood estimation (Martins and Stedinger, 2000), L-moment estimates. The comparison of FFCs from different rainfall forcings lead to the same conclusion for both seasons and both time scales.

4.3 Insights on catchment runoff generation

To understand how the generated rainfall results in an inadequate behaviour of hourly peak discharge, particularly in summer, the fractions of saturated soil for different rainfall forcing are compared. Then the impact of spatial rainfall structure on the spatial pattern of soil moisture is assessed. In JJA (river Welland), the NS(s-t) forcing gives an overall lower fraction of saturated

soil, compared with the observed fraction of saturated soil (Fig. 9). The discrepancy becomes more significant with increasing mean areal intensity. In DJF, the resulting soil pattern from the NS(s-t) forcing is in closer agreement with the one from observed rainfall forcing.

The lower areal fraction of saturated soil is due to the wet area ratio being underestimated by the stochastic model (Fig. 6.c). The lower areal fraction of saturated soil is pronounced in JJA, but less significant in DJF. It might be related to an additive effect of storm movement (advection) in the observed summer rainfall. With the movement, a larger area will be saturated, something which is not well captured by the model. Simplified static storms with the same intensity in the rainfall model lead to higher spatial connectivity of surface water transport. Therefore, the excess flow is able to travel faster into the river channel and results in a faster and more intense catchment response (Paschalis et al., 2014a; Seo et al., 2012). It suggests that the rain cell structure plays an important role in the spatial distribution of saturated soil moisture, which is directly linked with the spatial distribution of generated excess runoff in river catchments.

5 Conclusions and Outlook

In summary, this study shows that the rainfall model reproduces most of key statistics of rainfall. Those statistics include moment estimates (up to the third order) of the marginal distribution of rainfall intensity, the autocorrelation of intensities, point rainfall extremes and the decay of spatial correlation with distance at both hourly and daily scales. However, the spatial correlation is generally overestimated at short distances, and the hourly areal extremes at the spatial scales of medium-sized catchments (~700 km^2) are also mostly overestimated. After a non-linear rainfall-runoff transformation, the overall distribution of flow series is preserved by the generated rainfall field in both high and low flow seasons. The daily peak flow during winter season is well captured with a relative bias of 4.79% on average at a 10-year return level.

Moving to hourly resolution, at the same return level, the model gives a comparable peak discharge with the reference runoff in winter but an overestimation of 163.5% in summer. The divergent performance in the two seasons is in agreement with the inadequately reproduced area of saturated soil during summer, which could be explained by the underestimated wet area ratio and the absence of storm movement in the rainfall model.

This conclusion is only based upon examining one of the state-of-the-art point-process models. The simplified spatial structure (no storm advection, spatially constant inner-cell intensity, lack of dependency between cell radius and intensity) is however essentially the same as that of the widely used version of this type of Neyman-Scott spatial-temporal model (Burton et al., 2008; Cowpertwait, 2006). The models could be improved by deriving the analytical solutions for a new point process model removing those assumptions, although there are only few attempts in this direction (Evin and Favre, 2008), because of the nearly intractable mathematical equations this gives rise to. Other point process models sharing this simplified spatial structure, would most likely also misrepresent the wet area ratio and overestimate the hourly areal extremes. Therefore, the conclusion in terms of the overestimated hourly peak discharge during the summer season can be generalised to most of the existing space-time models based on point processes and sharing these assumptions. The misrepresentation could be greater for applications of the model to locations experiencing more frequent convective events.

Aside from the intrinsic model structure, the shortcoming of this point process model for catchment studies is related to its calibration procedure. Certain key descriptors of the rainfall for river flood estimation could not be used in calibrating the NS(s-t) model under the GMM. This is the case for example, for the total areal rainfall over the catchment, or accumulated rainfall depth over a storm event. A potential solution is to consider a calibration method involving

simulations, so that we could consider directly calibrating rainfall models to the areal rainfall, even runoff statistics. For example, one approach for this calibration method would be to use a likelihood free method such as Approximate Bayesian Computation instead of using a GMM-based calibration. Such calibration methods place no restrictions on what statistics can be used, but they come at the expense of an enormous computational cost. Compared with other weather generators (such as Serinaldi and Kilsby, 2014, fig. 13; Tarpanelli et al., 2012, fig. 10), these models converge in their overestimation of areal extremes at the desired temporal resolution. A careful check on generated areal rainfall amount by a rainfall generator will be essential for future applications.

In future research more complex models might be needed for a better estimation of catchment hydrological responses. Whether the model we used here or another type of space-time models (such as Gires et al., 2012; Papalexiou, 2018; Paschalis et al., 2013) performs better remains an open question. Further research could explore how the choice of stochastic rainfall model affects the generated rainfall and catchment response.

Regarding the implications for real world case studies, the stochastic rainfall model can be used to obtain flood frequency curves, by using an ensemble of simulations so as to represent the stochastic uncertainty. We have shown that this type of stochastic rainfall can produce a long-term flow comparable at both daily and hourly scales with the reference runoff with observed rainfall forcing. It implies that point process models are suitable for obtaining flow duration curves, and particularly well-behaved for high flow seasons. The well simulated daily peak discharge confirms the model's validity in inferring the flood frequency curves at ungauged sites at a daily scale. However, the model is not suitable for obtaining hourly flood frequency curves, particularly during the summer season, because the peak discharge can be largely overestimated.

This overestimation could lead to unnecessary investments in flood mitigation measures. Note that our study focuses on river flooding; we did not consider the potential risk of other flooding types such as groundwater flooding due to high groundwater levels (DEFRA, 2009b).

Acknowledgments, Samples, and Data

Rain gauge data were provided by Anglian Water (https://www.anglianwater.co.uk/). Weather radar data were provided by UK Met Office, available through the British Atmospheric Data Centre (http://catalogue.ceda.ac.uk/uuid/27dd6ffba67f667a18c62de5c3456350). CEH-GEAR data were downloaded from UK Centre for Ecology & Hydrology (https://doi.org/10.5285/ee9ab43d-a4fe-4e73-afd5-cd4fc4c82556). CHESS-PE data were downloaded from UK Centre for Ecology & Hydrology (https://doi.org/10.5285/8baf805d-39ce-4dac-b224-c926ada353b7). Stream flow observation were obtained from National River Flow Archive of UK (https://nrfa.ceh.ac.uk/). Soil data were downloaded from SoilGrids (https://soilgrids.org/#!/?layer=ORCDRC_M_sl2_250m&vector=1). OS Terrain 50 data were provided by the Ordnance Survey, downloaded from Digimap (https://digimap.edina.ac.uk/). Hydrological Modelling tool was provided by Dr Fatichi (ETH Zurich, National University of Singapore)

References

Andrés-Doménech, I., García-Bartual, R., Montanari, A., Marco, J.B., 2015. Climate and hydrological variability: the catchment filtering role. Hydrology and Earth System Sciences 19, 379–387. https://doi.org/10.5194/hess-19-379-2015

Anstead, L., Tovey, N.K., 2017. Hydrological and geomorphological challenges of water transfers in East Anglia, UK in the context of climate change. International Journal of Water 11, 14. https://doi.org/10.1504/IJW.2017.081108

Bell, F.C., 1976. The areal reduction factor in rainfall frequency estimation. Institute of Hydrology, Wallingford.

Bell, T.L., 1987. A space-time stochastic model of rainfall for satellite remote-sensing studies 9631.

Bell, V.A., Kay, A., Jones, R.G., Moore, R.J., 2007. Development of a high resolution grid-based river flow model for use with regional climate model output. Hydrology and Earth System Sciences 11, 532–549. https://doi.org/10.5194/hess-11-532-2007

Benettin, P., Kirchner, J.W., Rinaldo, A., Botter, G., 2015. Modeling chloride transport using travel time distributions at Plynlimon, Wales. Water Resources Research 51, 3259–3276. https://doi.org/10.1002/2014WR016600

Biggs, E.M., Atkinson, P.M., 2011. A comparison of gauge and radar precipitation data for simulating an extreme hydrological event in the Severn Uplands, UK. Hydrological Processes 25, 795–810. https://doi.org/10.1002/hyp.7869

Blenkinsop, S., Lewis, E., Chan, S.C., Fowler, H.J., 2017. Quality- control of an hourly rainfall dataset and climatology of extremes for the UK. International Journal of Climatology 37, 722–740. https://doi.org/10.1002/joc.4735

Brath, A., Montanari, A., Moretti, G., 2006. Assessing the effect on flood frequency of land use change via hydrological simulation (with uncertainty). Journal of Hydrology 324, 141–153. https://doi.org/10.1016/j.jhydrol.2005.10.001

Breinl, K., Müller-Thomy, H., Blöschl, G., 2020. Space–Time Characteristics of Areal Reduction Factors and Rainfall Processes. Journal of Hydrometeorology 21, 671–689. https://doi.org/10.1175/JHM-D-19-0228.1

Burton, A., Fowler, H.J., Kilsby, C.G., O'Connell, P.E., 2010. A stochastic model for the spatial-temporal simulation of nonhomogeneous rainfall occurrence and amounts. Water Resources Research 46. https://doi.org/10.1029/2009WR008884

Burton, A., Kilsby, C.G., Fowler, H.J., Cowpertwait, P.S.P., O'Connell, P.E., 2008. RainSim: A spatial–temporal stochastic rainfall modelling system. Environmental Modelling and Software 23, 1356–1369. https://doi.org/10.1016/j.envsoft.2008.04.003

Callau Poduje, A.C., Haberlandt, U., 2017. Short time step continuous rainfall modeling and simulation of extreme events. Journal of Hydrology 552, 182–197. https://doi.org/https://doi.org/10.1016/j.jhydrol.2017.06.036

Cameron, D., Beven, K., Tawn, J., 2000. An evaluation of three stochastic rainfall models. Journal of Hydrology 228, 130–149. https://doi.org/https://doi.org/10.1016/S0022-1694(00)00143-8

Camici, S., Brocca, L., Melone, F., Moramarco, T., 2014. Impact of Climate Change on Flood Frequency Using Different Climate Models and Downscaling Approaches. Journal of Hydrologic Engineering 19, 4014002. https://doi.org/10.1061/(ASCE)HE.1943-5584.0000959

Chen, Y., Paschalis, A., Kendon, E., Kim, D., Onof, C., 2021. Changing Spatial Structure of Summer Heavy Rainfall, Using Convection-Permitting Ensemble. Geophysical Research Letters 48, e2020GL090903. https://doi.org/https://doi.org/10.1029/2020GL090903

Coles, S., 2013. An Introduction to Statistical Modeling of Extreme Values, Springer Series in Statistics. Springer London, Limited, London. https://doi.org/10.1007/978-1-4471-3675-0

Courant, R., Friedrichs, K., Lewy, H., 1928. Über die partiellen Differenzengleichungen der mathematischen Physik. Mathematische Annalen 100, 32–74. https://doi.org/10.1007/BF01448839

Cowpertwait, P.S.P., 2010. A spatial- temporal point process model with a continuous distribution of storm types. Water Resources Research 46, n/a. https://doi.org/10.1029/2010WR009728

Cowpertwait, P.S.P., 2006. A spatial–temporal point process model of rainfall for the Thames catchment, UK. Journal of Hydrology 330, 586–595. https://doi.org/10.1016/j.jhydrol.2006.04.043

Cowpertwait, P.S.P., 2004. Mixed rectangular pulses models of rainfall. Hydrology and Earth System Sciences 8, 993–1000. https://doi.org/10.5194/hess-8-993-2004

Cowpertwait, P.S.P., 1995. A Generalized Spatial-Temporal Model of Rainfall Based on a Clustered Point Process. Proceedings of the Royal Society of London. Series A: Mathematical and Physical Sciences 450, 163–175. https://doi.org/10.1098/rspa.1995.0077
Cowpertwait, P.S.P., 1994. A Generalized Point Process Model for Rainfall. Proceedings of the Royal Society of London. Series A: Mathematical and Physical Sciences 447, 23–37. https://doi.org/10.1098/rspa.1994.0126
Cowpertwait, P.S.P., Kilsby, C., O'Connell, P., 2002. A space-time Neyman-Scott model of rainfall: Empirical analysis of extremes. Water Resources Research 38, 6–14. https://doi.org/10.1029/2001WR000709
Cowpertwait, P.S.P., Ocio, D., Collazos, G., de Cos, O., Stocker, C., 2013. Regionalised spatiotemporal rainfall and temperature models for flood studies in the Basque Country, Spain. Hydrology and Earth System Sciences 17, 479–494. https://doi.org/10.5194/hess-17-479-2013
Cristiano, E., ten Veldhuis, J.A.E., van de Giesen, N.C., 2017. Spatial and temporal variability of rainfall and their effects on hydrological response in urban areas - A review. Hydrology and Earth System Sciences 21, 3859–3878. https://doi.org/10.5194/hess-21-3859-2017
Cunha, L.K., Mandapaka, P. v, Krajewski, W.F., Mantilla, R., Bradley, A.A., 2012. Impact of radar- rainfall error structure on estimated flood magnitude across scales: An investigation based on a parsimonious distributed hydrological model. Water Resources Research 48, n/a. https://doi.org/10.1029/2012WR012138
DEFRA, 2016a. Anglian river basin district flood risk management plan, Department for Environment, Food and Rural Affairs. Environment Agency.
DEFRA, 2016b. Anglian River Basin District Flood Risk Management Plan 2015 - 2021 PART B – Sub Areas in the Anglian River Basin District, Department for Environment, Food and Rural Affairs.
DEFRA, 2009a. North Essex: Catchment Flood Management Plan, Department for Environment, Food and Rural Affairs. Environment Agency.
DEFRA, 2009b. River Welland: Catchment flood management plan, Department for Environment, Food and Rural Affairs. Environment Agency.
Environment Agency, 2016. The costs and impacts of the winter 2013 to 2014 floods, Department for Environment, Food and Rural Affairs. Environment Agency.
Evin, G., Favre, A.-C., 2008. A new rainfall model based on the Neyman-Scott process using cubic copulas. Water Resources Research 44. https://doi.org/10.1029/2007WR006054
Fatichi, S., Ivanov, V.Y., Paschalis, A., Peleg, N., Molnar, P., Rimkus, S., Kim, J., Burlando, P., Caporali, E., 2016. Uncertainty partition challenges the predictability of vital details of climate change. Earth's Future 4, 240–251. https://doi.org/10.1002/2015EF000336
Faurès, J.-M., Goodrich, D.C., Woolhiser, D.A., Sorooshian, S., 1995. Impact of small-scale spatial rainfall variability on runoff modeling. Journal of Hydrology 173, 309–326. https://doi.org/10.1016/0022-1694(95)02704-S
Felder, G., Weingartner, R., 2016. An approach for the determination of precipitation input for worst-case flood modelling. Hydrological Sciences Journal 61, 2600–2609. https://doi.org/10.1080/02626667.2016.1151980
Gires, A., Onof, C., Maksimovic, C., Schertzer, D., Tchiguirinskaia, I., Simoes, N., 2012. Quantifying the impact of small scale unmeasured rainfall variability on urban runoff through multifractal downscaling: A case study. Journal of Hydrology 442–443, 117–128. https://doi.org/10.1016/j.jhydrol.2012.04.005
Gray, M.E.B., Marshall, C., 1998. Mesoscale convective systems over the UK, 1981–97. Weather 53, 388–396. https://doi.org/10.1002/j.1477-8696.1998.tb06352.x
Hardenberg, J. v, Ferraris, L., Provenzale, A., 2003. The shape of convective rain cells. Geophysical Research Letters 30, 2280-n/a. https://doi.org/10.1029/2003GL018539
Harrigan, S., Hannaford, J., Muchan, K., Marsh, T.J., 2018. Designation and trend analysis of the updated UK Benchmark Network of river flow stations: the UKBN2 dataset. Hydrology Research 49, 552–567. https://doi.org/10.2166/nh.2017.058
Hengl, T., 2018a. Clay Content In % (Kg / Kg) At 6 Standard Depths (0, 10, 30, 60, 100 And 200 Cm) At 250 M Resolution (Version v0.2). https://doi.org/10.5281/zenodo.1476855
Hengl, T., 2018b. Sand Content In % (Kg / Kg) At 6 Standard Depths (0, 10, 30, 60, 100 And 200 Cm) At 250 M Resolution (Version v0.2). https://doi.org/10.5281/zenodo.1476852
Hengl, T., Wheeler, I., 2018. Soil Organic Carbon Content In X 5 G / Kg At 6 Standard Depths (0, 10, 30, 60, 100 And 200 Cm) At 250 M Resolution (Version v0.2). https://doi.org/10.5281/zenodo.1475458
Jesus, J., Chandler, R.E., 2011. Estimating functions and the generalized method of moments. Interface focus 1, 871–885. https://doi.org/10.1098/rsfs.2011.0057
Kaczmarska, J., Isham, V., Onof, C., 2014. Point process models for fine-resolution rainfall. Hydrological Sciences Journal 59, 1972–1991. https://doi.org/10.1080/02626667.2014.925558

Kay, A., Davies, H.N., Bell, V.A., Jones, R.G., 2009. Comparison of uncertainty sources for climate change impacts: flood frequency in England. Climatic Change 92, 41–63. https://doi.org/10.1007/s10584-008-9471-4
Kay, A., Rudd, A., Davies, H., Kendon, E., Jones, R., 2015. Use of very high resolution climate model data for hydrological modelling: baseline performance and future flood changes. Climatic Change 133, 193–208. https://doi.org/10.1007/s10584-015-1455-6
Kendon, E.J., Roberts, N.M., Senior, C.A., Roberts, M.J., 2012. Realism of Rainfall in a Very High-Resolution Regional Climate Model. Journal of Climate 25, 5791–5806. https://doi.org/10.1175/JCLI-D-11-00562.1
Lamb, R., Faulkner, D., Zaidman, M., 2010. Fluvial Design Guide, Environment Agency. Environment Agency, UK.
Lavers, D.A., Allan, R.P., Wood, E.F., Villarini, G., Brayshaw, D.J., Wade, A.J., 2011. Winter floods in Britain are connected to atmospheric rivers. Geophysical Research Letters 38, n/a. https://doi.org/10.1029/2011GL049783
Leonard, M., Lambert, M.F., Metcalfe, A. v, Cowpertwait, P.S.P., 2008. A space-time Neyman-Scott rainfall model with defined storm extent. Water Resources Research 44. https://doi.org/10.1029/2007WR006110
Lewis, M.W., Gray, S.L., 2010. Categorisation of synoptic environments associated with mesoscale convective systems over the UK. Atmospheric Research. https://doi.org/https://doi.org/10.1016/j.atmosres.2010.04.001
Lobligeois, F., Andréassian, V., Perrin, C., Tabary, P., Loumagne, C., 2014. When does higher spatial resolution rainfall information improve streamflow simulation? An evaluation using 3620 flood events. Hydrology and Earth System Sciences 18, 575–594. https://doi.org/10.5194/hess-18-575-2014
Mandapaka, P. v, Krajewski, W.F., Mantilla, R., Gupta, V.K., 2009. Dissecting the effect of rainfall variability on the statistical structure of peak flows. Advances in Water Resources 32, 1508–1525. https://doi.org/https://doi.org/10.1016/j.advwatres.2009.07.005
Martins, E.S., Stedinger, J.R., 2000. Generalized maximum-likelihood generalized extreme-value quantile estimators for hydrologic data. Water Resources Research 36, 737–744. https://doi.org/https://doi.org/10.1029/1999WR900330
McRobie, F.H., Wang, L.-P., Onof, C., Kenney, S., 2013. A spatial-temporal rainfall generator for urban drainage design. Water science and technology : a journal of the International Association on Water Pollution Research 68, 240–249. https://doi.org/10.2166/wst.2013.241
Melsen, L., Teuling, A., Torfs, P., Zappa, M., Mizukami, N., Clark, M., Uijlenhoet, R., 2016. Representation of spatial and temporal variability in large-domain hydrological models: case study for a mesoscale pre-Alpine basin. Hydrology and Earth System Sciences 20, 2207–2226. https://doi.org/10.5194/hess-20-2207-2016
Met Office, 2016. Technical note: Issue with UKCP Local (2.2km) simulation data [WWW Document]. URL https://www.metoffice.gov.uk/binaries/content/assets/metofficegovuk/pdf/weather/learn-about/uk-past-events/regional-climates/eastern-england_-climate---met-office.pdf (accessed 10.2.20).
Met Office, 2003. Met Office Rain Radar Data from the NIMROD System. NCAS British Atmospheric Data Centre [WWW Document].
Monteith, J.L., 1965. Evaporation and environment. Symposia of the Society for Experimental Biology 19, 205—234.
Moretti, G., Montanari, A., 2008. Inferring the flood frequency distribution for an ungauged basin using a spatially distributed rainfall-runoff model. Hydrology and Earth System Sciences 12, 1141–1152. https://doi.org/10.5194/hess-12-1141-2008
Müller-Thomy, H., Wallner, M., Förster, K., 2018. Rainfall disaggregation for hydrological modeling: is there a need for spatial consistence? Hydrology and Earth System Sciences 22, 5259–5280. https://doi.org/10.5194/hess-22-5259-2018
Nash, J.E., Sutcliffe, J. v, 1970. River flow forecasting through conceptual models part I — A discussion of principles. Journal of Hydrology 10, 282–290. https://doi.org/10.1016/0022-1694(70)90255-6
Neal, R.A., Phillips, I.D., 2009. Summer daily precipitation variability over the East Anglian region of Great Britain. International Journal of Climatology 29, 1661–1679. https://doi.org/10.1002/joc.1826
Nicótina, L., Alessi Celegon, E., Rinaldo, A., Marani, M., 2008. On the impact of rainfall patterns on the hydrologic response. Water Resources Research 44. https://doi.org/10.1029/2007WR006654
Northrop, P., 1998. A clustered spatial-temporal model of rainfall. Proceedings of the Royal Society of London. Series A: Mathematical, Physical and Engineering Sciences 454, 1875–1888. https://doi.org/10.1098/rspa.1998.0238
NRFA, 2019a. Stour at Stratford St Mary [WWW Document]. URL https://nrfa.ceh.ac.uk/data/station/info/36001
NRFA, 2019b. Gauged Daily Flow Data [WWW Document]. URL https://nrfa.ceh.ac.uk

Ochoa- Rodriguez, S., Wang, L., Willems, P., Onof, C., 2019. A review of radar- rain gauge data merging methods and their potential for urban hydrological applications. https://doi.org/10.1029/2018WR023332
Ochoa-Rodriguez, S., Wang, L.-P., Gires, A., Pina, R.D., Reinoso-Rondinel, R., Bruni, G., Ichiba, A., Gaitan, S., Cristiano, E., van Assel, J., Kroll, S., Murlà-Tuyls, D., Tisserand, B., Schertzer, D., Tchiguirinskaia, I., Onof, C., Willems, P., ten Veldhuis, M.-C., 2015. Impact of spatial and temporal resolution of rainfall inputs on urban hydrodynamic modelling outputs: A multi-catchment investigation. Journal of Hydrology 531, 389–407. https://doi.org/10.1016/j.jhydrol.2015.05.035
Onof, C., Chandler, R., Kakou, A., Northrop, P., Wheater, H., Isham, V., 2000. Rainfall modelling using Poisson-cluster processes: a review of developments. Stochastic Environmental Research and Risk Assessment 14, 384. https://doi.org/10.1007/s004770000043
Onof, C., Wang, L.-P., 2020. Modelling rainfall with a Bartlett–Lewis process: new developments. Hydrology and Earth System Sciences 24, 2791–2815. https://doi.org/10.5194/hess-24-2791-2020
Onof, C., Wheater, H., 1994. Improvements to the modelling of British rainfall using a modified Random Parameter Bartlett-Lewis Rectangular Pulse Model. Journal of hydrology 157, 177–195.
Ordnance Survey, 2018. OS MasterMap Topography Layer - OS Terrain 50 [WWW Document]. URL https://digimap.edina.ac.uk/roam/download/os
Over, T.M., Gupta, V.K., 1996. A space- time theory of mesoscale rainfall using random cascades. Journal of Geophysical Research: Atmospheres 101, 26319–26331. https://doi.org/10.1029/96JD02033
Papalexiou, S.M., 2018. Unified theory for stochastic modelling of hydroclimatic processes: Preserving marginal distributions, correlation structures, and intermittency. Advances in Water Resources 115, 234–252. https://doi.org/10.1016/j.advwatres.2018.02.013
Park, J., Onof, C., Kim, D., 2019. A hybrid stochastic rainfall model that reproduces some important rainfall characteristics at hourly to yearly timescales. Hydrology and Earth System Sciences 23, 989–1014. https://doi.org/10.5194/hess-23-989-2019
Paschalis, A., Fatichi, S., Molnar, P., Rimkus, S., Burlando, P., 2014a. On the effects of small scale space–time variability of rainfall on basin flood response. Journal of Hydrology 514, 313–327. https://doi.org/10.1016/j.jhydrol.2014.04.014
Paschalis, A., Molnar, P., Fatichi, S., Burlando, P., 2014b. On temporal stochastic modeling of precipitation, nesting models across scales. Advances in Water Resources 63, 152–166. https://doi.org/10.1016/j.advwatres.2013.11.006
Paschalis, A., Molnar, P., Fatichi, S., Burlando, P., 2013. A stochastic model for high- resolution space- time precipitation simulation. Water Resources Research 49, 8400–8417. https://doi.org/10.1002/2013WR014437
Peleg, N., Blumensaat, F., Molnar, P., Fatichi, S., Burlando, P., 2017a. Partitioning the impacts of spatial and climatological rainfall variability in urban drainage modeling. Hydrology and Earth System Sciences 21, 1559–1572. https://doi.org/10.5194/hess-21-1559-2017
Peleg, N., Fatichi, S., Paschalis, A., Molnar, P., Burlando, P., 2017b. An advanced stochastic weather generator for simulating 2-D high-resolution climate variables. Journal of Advances in Modeling Earth Systems 9, 1595–1627. https://doi.org/10.1002/2016MS000854
Porporato, A., Laio, F., Ridolfi, L., Rodriguez-Iturbe, I., 2001. Plants in water-controlled ecosystems: active role in hydrologic processes and response to water stress: III. Vegetation water stress. Advances in Water Resources 24, 725–744. https://doi.org/10.1016/S0309-1708(01)00006-9
Prein, A.F., Langhans, W., Fosser, G., Ferrone, A., Ban, N., Goergen, K., Keller, M., Tölle, M., Gutjahr, O., Feser, F., Brisson, E., Kollet, S., Schmidli, J., Lipzig, N.P.M., Leung, R., 2015. A review on regional convection-permitting climate modeling: Demonstrations, prospects, and challenges. Reviews of Geophysics 53, 323–361. https://doi.org/10.1002/2014RG000475
Prudhomme, C., Reynard, N., Crooks, S., 2002. Downscaling of global climate models for flood frequency analysis: where are we now? Hydrological Processes 16, 1137–1150. https://doi.org/10.1002/hyp.1054
Ralph, F.M., Neiman, P.J., Wick, G.A., Gutman, S.I., Dettinger, M.D., Cayan, D.R., White, A.B., 2006. Flooding on California's Russian River: Role of atmospheric rivers. Geophysical Research Letters 33. https://doi.org/10.1029/2006GL026689
Ramesh, N.I., Thayakaran, R., Onof, C., 2013. Multi-site doubly stochastic Poisson process models for fine-scale rainfall. Stochastic Environmental Research and Risk Assessment 27, 1383–1396. https://doi.org/10.1007/s00477-012-0674-x
Ran, Q., Su, D., Li, P., He, Z., 2012. Experimental study of the impact of rainfall characteristics on runoff generation and soil erosion. Journal of Hydrology 424–425, 99–111. https://doi.org/https://doi.org/10.1016/j.jhydrol.2011.12.035

Remondi, F., Kirchner, J.W., Burlando, P., Fatichi, S., 2018. Water Flux Tracking With a Distributed Hydrological Model to Quantify Controls on the Spatiotemporal Variability of Transit Time Distributions. Water Resources Research 54, 3081–3099. https://doi.org/10.1002/2017WR021689

Ritter, A., Muñoz-Carpena, R., 2013. Performance evaluation of hydrological models: Statistical significance for reducing subjectivity in goodness-of-fit assessments. Journal of Hydrology 480, 33–45. https://doi.org/10.1016/j.jhydrol.2012.12.004

Robinson, E.L., Blyth, E., Clark, D.B., Comyn-Platt, E., Finch, J., Rudd, A.C., 2016. Climate hydrology and ecology research support system potential evapotranspiration dataset for Great Britain (1961-2015) [CHESS-PE]. https://doi.org/10.5285/8baf805d-39ce-4dac-b224-c926ada353b7

Ruiz-Villanueva, V., Borga, M., Zoccatelli, D., Marchi, L., Gaume, E., Ehret, U., 2012. Extreme flood response to short-duration convective rainfall in South-West Germany. Hydrology and Earth System Sciences 16, 1543–1559. https://doi.org/10.5194/hess-16-1543-2012

Rulli, M.C., Rosso, R., 2002. An integrated simulation method for flash-flood risk assessment: 1. Frequency predictions in the Bisagno River by combining stochastic and deterministic methods. Hydrology and Earth System Sciences 6, 267–284. https://doi.org/10.5194/hess-6-267-2002

Saxton, K.E., Rawls, W.J., 2006. Soil Water Characteristic Estimates by Texture and Organic Matter for Hydrologic Solutions. Soil Science Society of America Journal 70, 1569. https://doi.org/10.2136/sssaj2005.0117

Segond, M.-L., Onof, C., 2009. Modelling of space–time rainfall for three UK regions. Proceedings of the Institution of Civil Engineers - Water Management 162, 147–158. https://doi.org/10.1680/wama.2009.162.2.147

Seo, Y., Schmidt, A.R., Sivapalan, M., 2012. Effect of storm movement on flood peaks: Analysis framework based on characteristic timescales. Water Resources Research 48, n/a. https://doi.org/10.1029/2011WR011761

Serinaldi, F., Kilsby, C.G., 2014. Simulating daily rainfall fields over large areas for collective risk estimation. Journal of Hydrology 512, 285–302. https://doi.org/https://doi.org/10.1016/j.jhydrol.2014.02.043

Sillmann, J., Kharin, V. v, Zhang, X., Zwiers, F.W., Bronaugh, D., 2013. Climate extremes indices in the CMIP5 multimodel ensemble: Part 1. Model evaluation in the present climate. Journal of Geophysical Research: Atmospheres 118, 1716–1733. https://doi.org/10.1002/jgrd.50203

Sordo-Ward, A., Bianucci, P., Garrote, L., Granados, A., 2016. The Influence of the Annual Number of Storms on the Derivation of the Flood Frequency Curve through Event-Based Simulation. Water 8, 335. https://doi.org/10.3390/w8080335

Svensson, C., Jones, D.A., 2010. Review of methods for deriving areal reduction factors. Journal of Flood Risk Management 3, 232–245. https://doi.org/10.1111/j.1753-318X.2010.01075.x

Tanguy, M., Dixon, H., Prosdocimi, I., Morris, D.G., Keller, V.D.J., 2019. Gridded estimates of daily and monthly areal rainfall for the United Kingdom (1890-2017) [CEH-GEAR]. https://doi.org/10.5285/ee9ab43d-a4fe-4e73-afd5-cd4fc4c82556

Tarpanelli, A., Franchini, M., Brocca, L., Camici, S., Melone, F., Moramarco, T., 2012. A simple approach for stochastic generation of spatial rainfall patterns. Journal of Hydrology 472–473, 63–76. https://doi.org/https://doi.org/10.1016/j.jhydrol.2012.09.010

Tetzlaff, D., Uhlenbrook, S., 2005. Significance of spatial variability in precipitation for process-oriented modelling: results from two nested catchments using radar and ground station data. Hydrology and Earth System Sciences 9, 29–41. https://doi.org/10.5194/hess-9-29-2005

Verhoest, N.E.C., Vandenberghe, S., Cabus, P., Onof, C., Meca- Figueras, T., Jameleddine, S., 2010. Are stochastic point rainfall models able to preserve extreme flood statistics? Hydrological Processes 24, 3439–3445. https://doi.org/10.1002/hyp.7867

Viglione, A., Chirico, G.B., Komma, J., Woods, R., Borga, M., Blöschl, G., 2010. Quantifying space-time dynamics of flood event types. Journal of Hydrology 394, 213–229. https://doi.org/10.1016/j.jhydrol.2010.05.041

Waymire, E.C., Gupta, V.K., 1993. A statistical analysis of mesoscale rainfall as a random cascade. Journal of Applied Meteorology 32, 251–267. https://doi.org/10.1175/1520-0450(1993)032%3C0251:ASAOMR%3E2.0.CO;2

Wheater, H., Chandler, R., Onof, C., Isham, V., Bellone, E., Yang, C., Lekkas, D., Lourmas, G., Segond, M.-L., 2005. Spatial-temporal rainfall modelling for flood risk estimation. Stochastic Environmental Research and Risk Assessment 19, 403–416. https://doi.org/10.1007/s00477-005-0011-8

Wheater, H., Isham, V.S., Chandler, R.E., Onof, C.J., Stewart, E.J., 2006. Improved methods for national spatial-temporal rainfall and evaporation modelling for BSM. Defra.

Winter, B., Schneeberger, K., Dung, N. v, Huttenlau, M., Achleitner, S., Stötter, J., Merz, B., Vorogushyn, S., 2019. A continuous modelling approach for design flood estimation on sub-daily time scale. Hydrological Sciences Journal 64, 539–554. https://doi.org/10.1080/02626667.2019.1593419

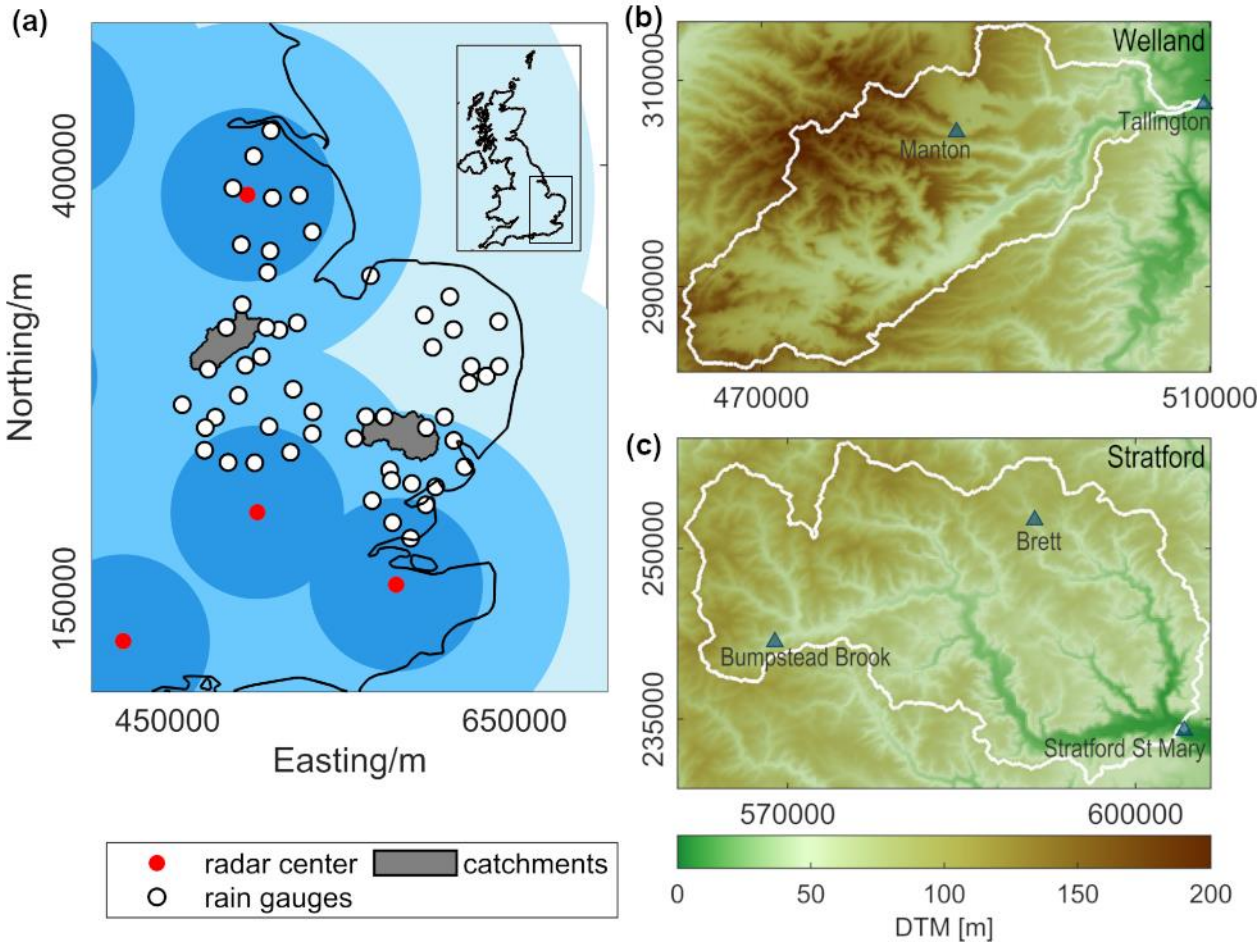


Figure 1. Location map of the study area, rain gauges and digital terrain model (DTM) of two experimental catchment areas. (a) locations of rain gauges, radar centre and two experimental catchment areas, the filled circles indicates distances of 50, 100 and 200km from the radar centre; (b,c) digital terrain model (DTM) of the Welland catchment with an outlet at Tallington and the Stour catchment with an outlet at Stratford St Mary

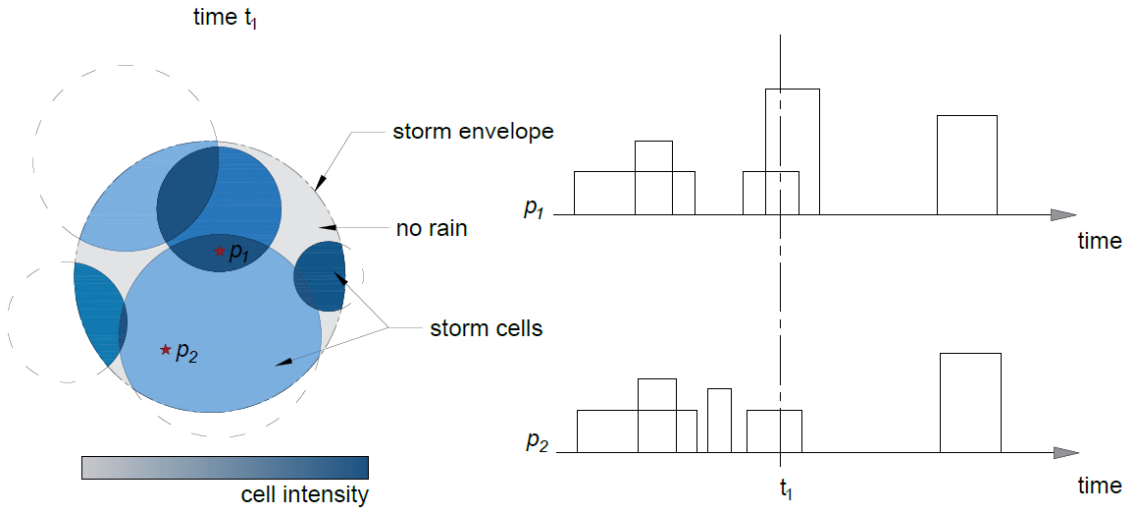


Figure 2. Schematic of the spatial-temporal rainfall model (left) the spatial pattern of time t_1, (right) the modelled cell occurrence at sites P_1 and P_2. The height of each rectangle represents the cell intensity. The length of each rectangle represents the cell duration.

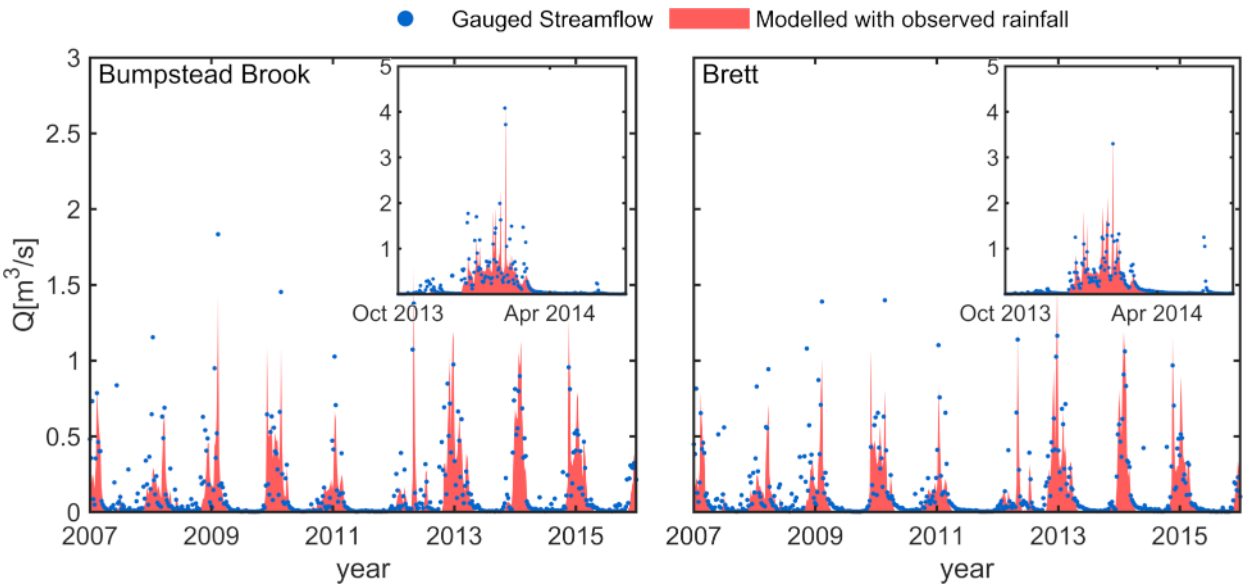


Figure 3. Comparison of long-term flow from observed gauges and model, at two benchmark stations. Enlargement of daily discharge between 2013 Oct and 2014 Jun in the box (top right of each plot).

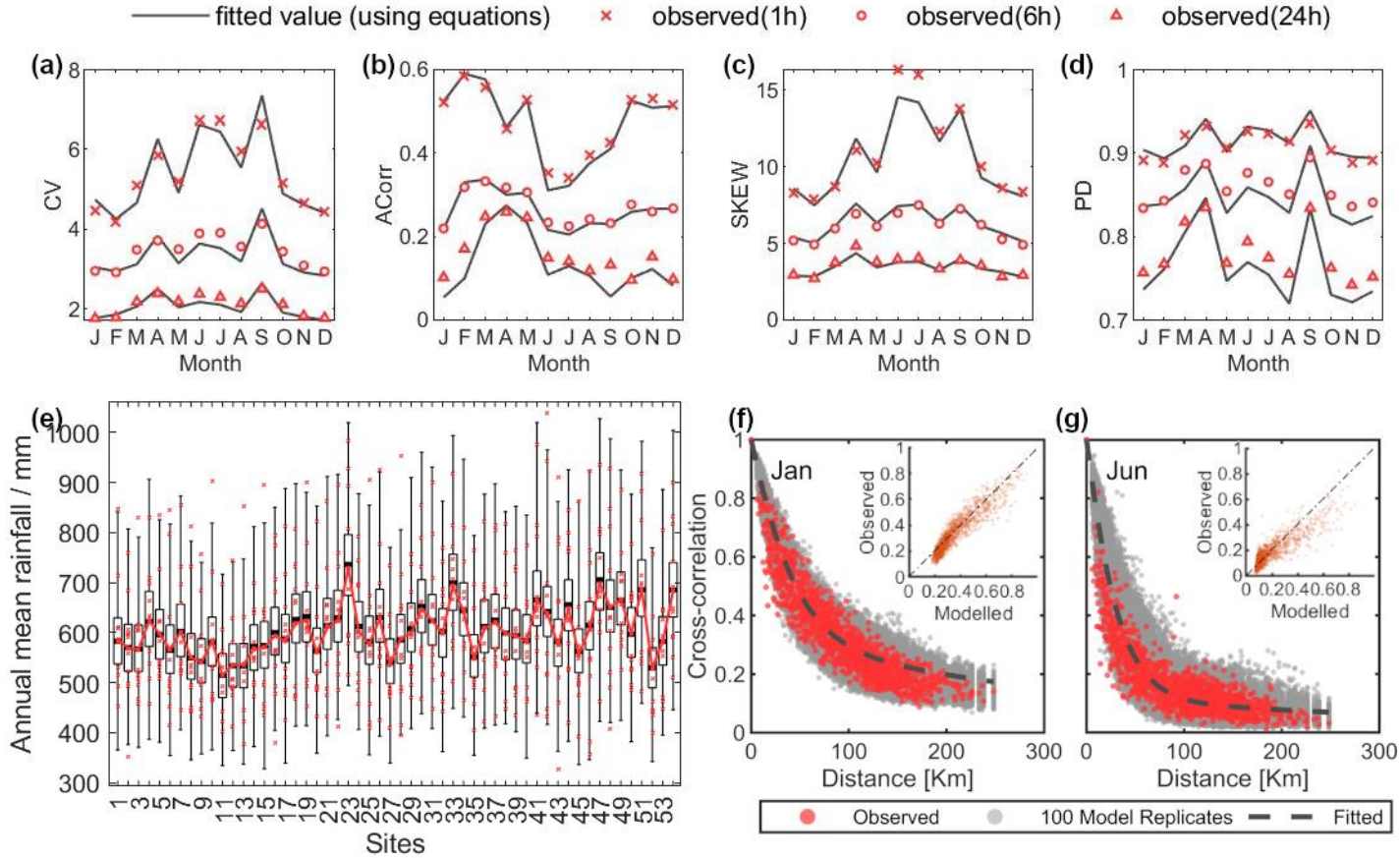


Figure 4. Validation of NS(s-t) model in terms of point rainfall statistics, including (a) coefficient of variation; (b) lag-1 autocorrelation; (c) coefficient of skewness; (d) probability of dry periods, at 1, 6, 24-hour aggregation levels; (e) annual mean daily rainfall: Red points represent the observed value which is the weighted average at 54 observation sites, the boxplots represent the range of 100 simulation replicates; (f, g) cross-correlation of hourly rainfall for all pairs of gauged sites in January and June, with a scatter plot between modelled and observed cross-correlations in the top right of each panel.

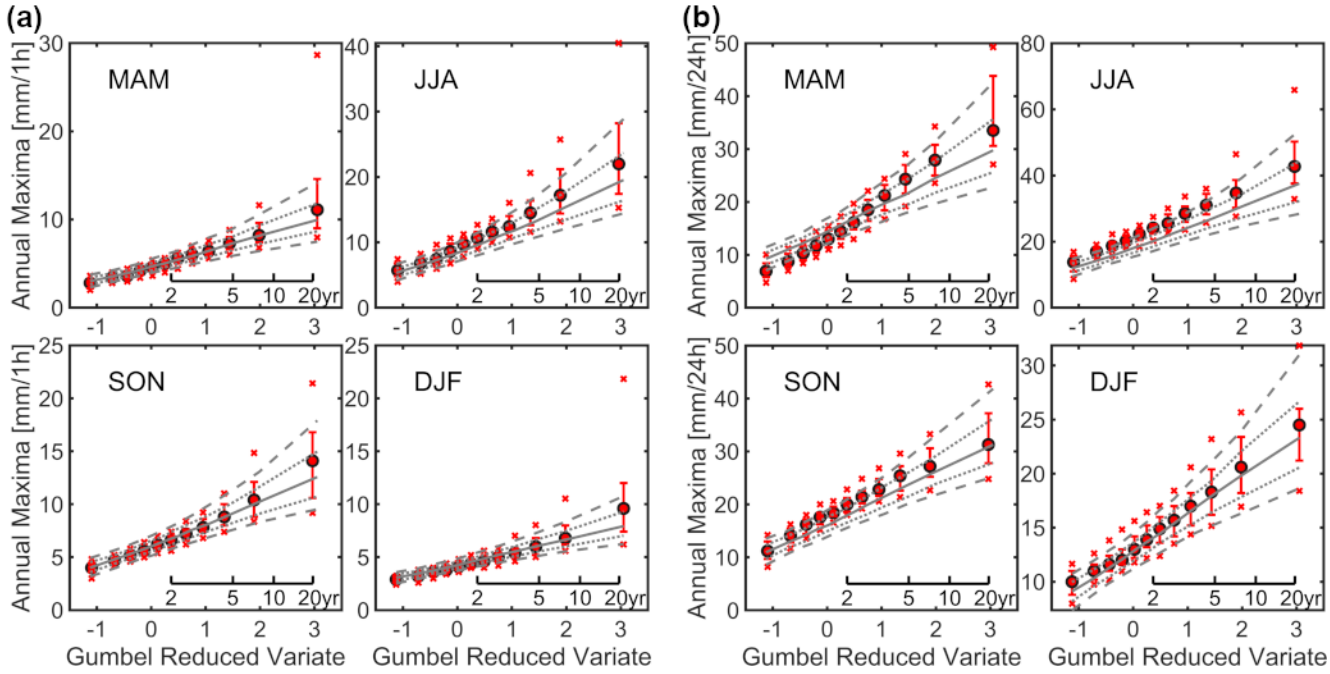


Figure 5. Annual maximum rainfall intensity against the return periods in different seasons, at (a) 1-hour aggregation level and (b) 24-hour aggregation level. The observed values are shown as quartile error bars, with upper and lower 10th percentiles shown as crosses and medians shown as circles. The solid line is an overall estimate (site-median, ensemble-median) for the simulated series. The dotted lines are estimates of the upper and lower quartiles, and the dashed lines are estimates of upper and lower 10 percentiles of data used to calculate the ordered medians (see method section for full explanation)

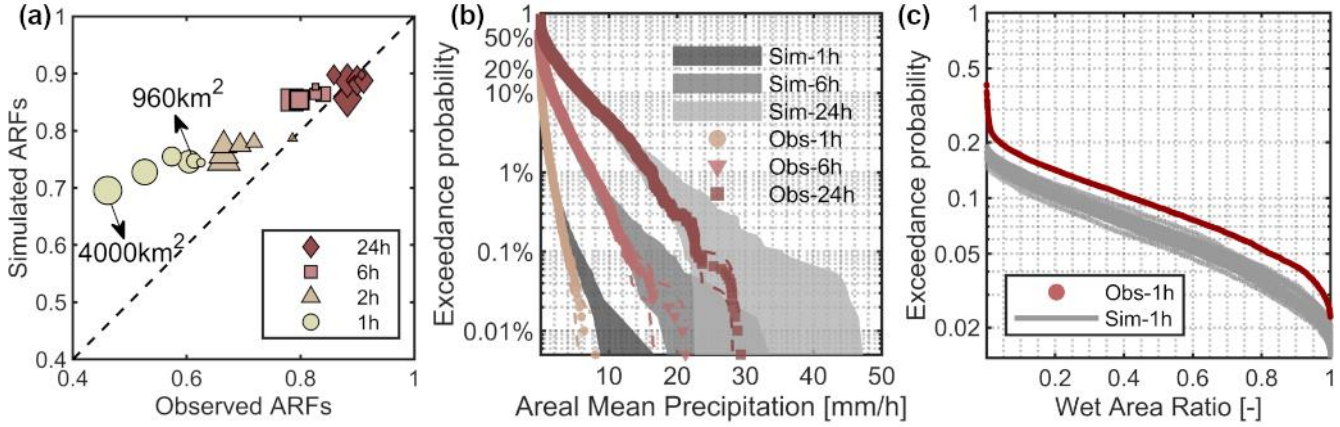


Figure 6. Comparison of modelled rain and observed rain on three statistics related to areal rainfall. (a) scatter plot of ARFs derived from (x-axis) radar observation and (y-axis) NS(s-t) generated field, for durations of 1,2,6 24 hours. The ARFs for several areas (400,960,1700,2600,3720 and 4000 km^2) were computed. Marker size indicates the magnitude of the aggregated area. (b) Exceedance probability of catchment rainfall at three aggregation levels (1, 6, 24 hours) for the Welland river catchment (717 km^2). (c) Exceedance probability of Wet Area Ratio (at Welland river catchment) at hourly scale for JJA.

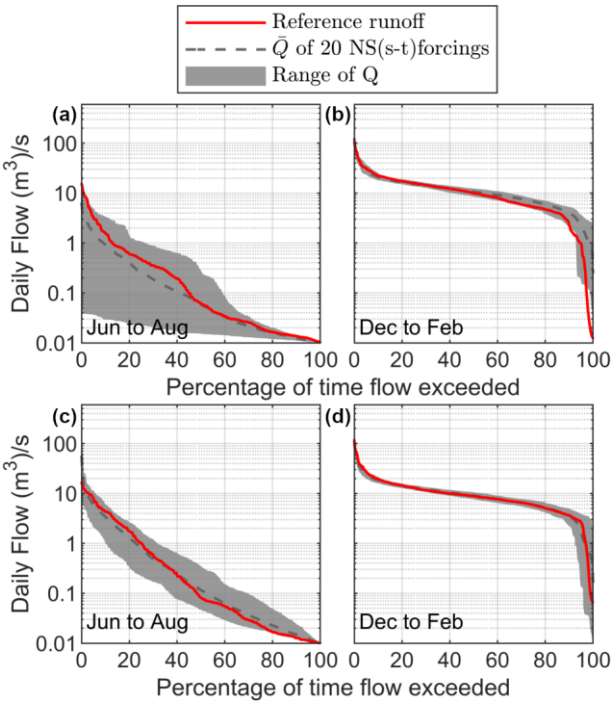


Figure 7. Comparison of flow duration curve between the reference runoff (simulation of observed rainfall forcing) and simulations of 20 NS(s-t) forcings at River Stour (a, b) and River Welland (c, d) catchments.

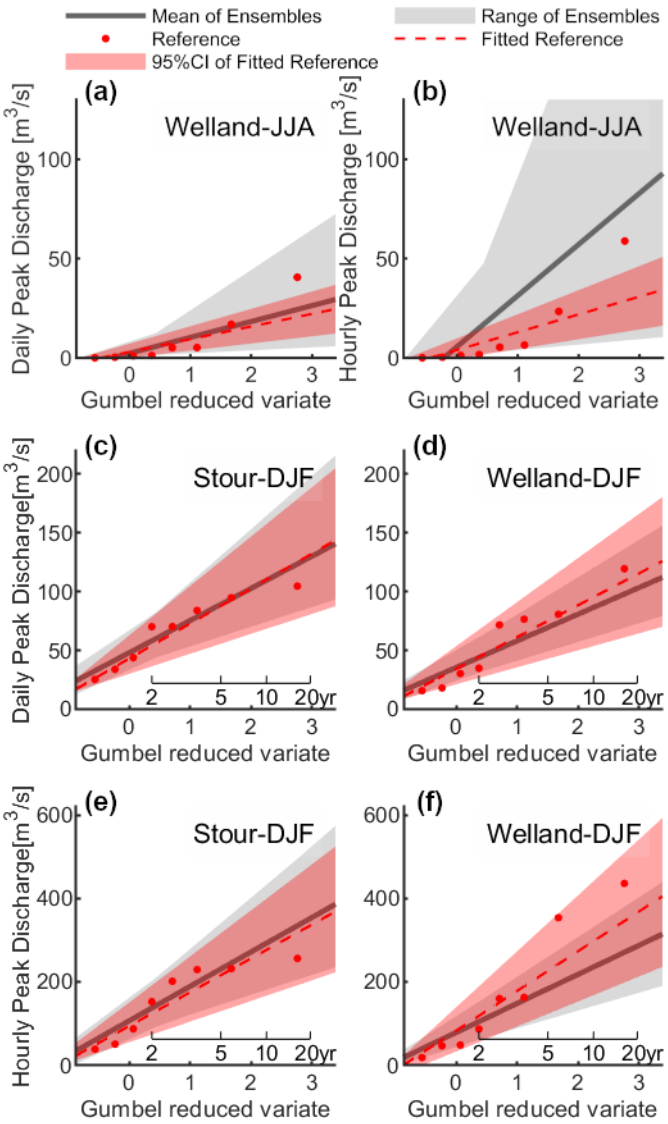


Figure 8. Comparisons of flood frequency curves (FFCs) from different rainfall forcings. (a, b) FFCs in summer season (JJA) at a daily and hourly scale respectively, (c, d) FFCs in winter season, at a daily scale; (e, f) FFCs in winter season (DJF), at an hourly scale. The shaded area of reference runoff (in red) gives a 95% confidence interval of Gumbel estimation of peak discharge. Shaded area in grey gives a range between 95th and 5th percentile of 20 ensemble simulation (Gumbel fitted).

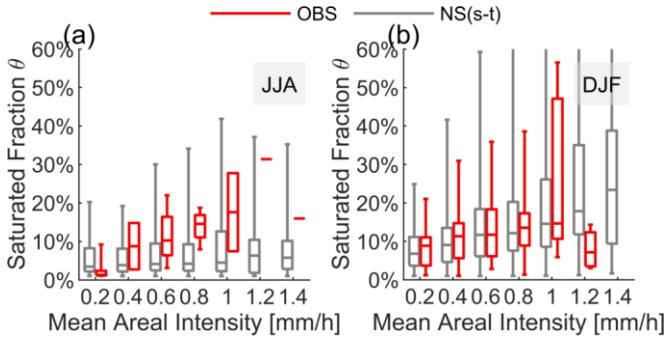


Figure 9. Saturated fraction of soil against the mean areal intensity in (a) JJA, (b) DJF at the River Welland Catchment. Mean areal intensity and the maximum saturated fraction were computed for each event conditioned on initial saturated fraction lower than 15%.

Table 1. Chosen Manning coef. and calibrated parameters of hydrological model for two catchments

Catchment property	Value
Manning Coef. - River	0.04 (McCuen, 2005, Table 3-4)
Manning Coef. - Arable	0.1 (McCuen, 2005, Table 3-4)
Anisotropy ratio	50
Root zone depth (mm)	450
Max Groundwater storage	1800
Exponent in storage-discharge function	2

Table 2. Relative error (month average) of summary statistics computed from the NS(s-t) model

Aggregation level	CV	SKEW	Acorr
1h	-0.64%	-3.37%	-2.14%
6h	-4.10%	3.60%	-2.26%
24h	-3.11%	-2.82%	-18.89%

* minus sign means underestimation.